

# Electroexcitation of the $P_{33}(1232)$ , $P_{11}(1440)$ , $D_{13}(1520)$ , and $S_{11}(1535)$ at $Q^2 = 0.4$ and $0.65$ ( $GeV/c$ )<sup>2</sup>

I.G. Aznauryan,<sup>1</sup> V.D. Burkert,<sup>2</sup> H. Egiyan,<sup>2</sup> K. Joo,<sup>3</sup> R. Minehart,<sup>4</sup> and L.C. Smith<sup>4</sup>

<sup>1</sup> *Yerevan Physics Institute, 375036 Yerevan, Armenia*

<sup>2</sup> *Thomas Jefferson National Accelerator Facility, Newport News, Virginia 23606*

<sup>3</sup> *University of Connecticut, Storrs, Connecticut 06269*

<sup>4</sup> *University of Virginia, Charlottesville, Virginia 22901*

Using two approaches: dispersion relations and isobar model, we have analyzed recent high precision CLAS data on cross sections of  $\pi^0$ ,  $\pi^+$ , and  $\eta$  electroproduction on protons, and the longitudinally polarized electron beam asymmetry for  $p(\vec{e}, e'p)\pi^0$  and  $p(\vec{e}, e'n)\pi^+$ . The contributions of the resonances  $P_{33}(1232)$ ,  $P_{11}(1440)$ ,  $D_{13}(1520)$ ,  $S_{11}(1535)$  to  $\pi$  electroproduction and  $S_{11}(1535)$  to  $\eta$  electroproduction are found. The results obtained in the two approaches are in good agreement. There is also good agreement between amplitudes of the  $\gamma^*N \rightarrow S_{11}(1535)$  transition found in  $\pi$  and  $\eta$  electroproduction. For the first time accurate results are obtained for the longitudinal amplitudes of the  $P_{11}(1440)$ ,  $D_{13}(1520)$ , and  $S_{11}(1535)$  electroexcitation on protons. A strong longitudinal response is found for the Roper resonance, which rules out presentation of this resonance as a hybrid state.

PACS numbers: PACS: 13.60.Le, 14.20.Gk, 11.55.Fv, 25.20.Lj, 25.30.Rw

## I. INTRODUCTION

The study of baryon structure is currently in a new stage of development as new data with unprecedented precision have become available due to the high intensity, high duty factor electron accelerators, complemented with large acceptance multi-particle detectors. Very precise measurements of electromagnetically induced hadron production and its  $Q^2$  evolution are available now, providing a new level in testing of phenomenological models and QCD in the nonperturbative and subasymptotic domains.

Much of our understanding of hadron structure is connected with the constituent quark model. Simple non-relativistic quark models were originally proposed and in many cases successfully used to explain the relations between the masses and photocouplings of hadrons. However, the picture is changing when  $Q^2$  grows, and successes of the simplified quark models do not extend to the electroexcitation amplitudes. Once the momentum transfer becomes greater than the masses of the constituent quarks, a relativistic treatment of the electromagnetic excitations becomes essential. The dependence on the small-distance interquark forces also becomes more significant with increasing  $Q^2$ . It is known also that a series of difficulties in the quark model description of the resonance properties, such as the unusually slow falloff with  $Q^2$  of the  $S_{11}(1535)$  transverse photocoupling amplitude and small mass of the  $P_{11}(1440)$ , gave rise to different explanations of the nature of the nucleon resonances. Among others, the presence of gluonic degrees of freedom in the  $P_{11}(1440)$  [1] and  $K\Sigma$  components in the  $S_{11}(1535)$  [2, 3] have been suggested. Accurate measurements of the resonance transition form factors will put all these models to stringent tests as the internal dynamics of excited states strongly affects their  $Q^2$  evolution.

It is remarkable that this new stage in the experimental

study of the  $Q^2$  evolution of the hadron electromagnetic characteristics is paralleled by the significant progress in lattice calculations and their successes in the description of the nucleon and transition form factors [4, 5, 6] and nucleon resonances masses [7]. Accurate results for the electroexcitation of the nucleon resonances will provide important information for understanding of the  $N^*$  structure from the first principles of QCD by exploring lattice calculations.

Recently, precise data on exclusive electroproduction of  $\pi^0$ ,  $\pi^+$ , and  $\eta$  on protons in the first and second resonance regions were obtained at Jefferson Lab using the CEBAF Large Acceptance Spectrometer (CLAS). The data include measurements of the cross sections [8, 9, 10], including complete angular distributions for the  $n\pi^+$  [9] and  $p\eta$  [10] final states. The data also include first measurements of the longitudinal beam asymmetry ( $A_{LT'}$ ) for  $p(\vec{e}, e'p)\pi^0$  [11] and  $p(\vec{e}, e'\pi^+)n$  [12].  $A_{LT'}$  is very sensitive to the interference of transverse and longitudinal amplitudes. These data allow one to investigate the contributions of resonances to  $\pi$  and  $\eta$  electroproduction in greater detail.

The goal of the present investigation is to extract from the data [8, 9, 10, 11, 12] the magnitudes of the  $P_{33}(1232)$ ,  $P_{11}(1440)$ ,  $D_{13}(1520)$  and  $S_{11}(1535)$  resonance contributions to these processes. The analysis is made using two approaches: (1) fixed-t dispersion relations (DR) and (2) isobar model (IM), which were both successfully used in Refs. [13, 14] to analyze  $\pi$  and  $\eta$  photoproduction. Comparison of the results obtained in the two conceptually very different approaches allows us to draw conclusions on the model dependence of the extracted resonance characteristics. The analysis was carried out at  $Q^2 = 0.4$  and  $0.65$  ( $GeV/c$ )<sup>2</sup>, where measurements of  $A_{LT'}$  were also made. For these values of  $Q^2$  we have available the most complete set of CLAS data on  $\pi^0$ ,  $\pi^+$ , and  $\eta$  cross sections. The formalism is presented

in Section II. In Section III we present the data and the method of analysis. In these Sections we also discuss the assumptions and approximations made in the analysis. In Section IV we present and discuss the results, and a comparison with previous data and quark model predictions is made. Finally, we summarize the results in Section V.

## II. THE ANALYSIS TOOLS

The approaches we use to analyze both  $\pi$  and  $\eta$  electroproduction on protons are dispersion relations and the isobar model approximation which are discussed in Refs. [13, 14] in detail. Here we only briefly present the main points of these approaches.

### A. Dispersion relations

The imaginary parts of the amplitudes in this approach are built from the  $s$  channel resonance contributions parametrized in the Breit-Wigner form. All four-, three-, and two-star resonances from the RPP [15] with masses up to 2.1  $GeV$  are taken into account. Using fixed- $t$  dispersion relations we find the real parts of the amplitudes. Real parts of the amplitudes include the Born term, i.e. the contributions of the nucleon poles in the  $s$  and  $u$  channels, and the contribution of the  $t$  channel  $\pi$  exchange in the case of pion electroproduction. They also include integrals over imaginary parts of the amplitudes, where we take into account only the contribution of the resonance energy region. According to estimations made in Refs. [13, 14], the role of the high energy contributions to dispersion integrals in the analysis of data in the first and second resonance regions is negligibly small.

In the case of pion electroproduction in the elasticity regions of multipole amplitudes, there is an additional constraint connected with the Watson theorem. According to the phase-shift analyses of the  $\pi N$  scattering, the  $\pi N$  amplitude  $h_{1+}^{3/2}$  is elastic up to  $W = 1.45 GeV$  (see, for example, the GWU(VPI) analysis [16, 17]). By this reason, utilization of the Watson theorem allows us to write dispersion relations for the amplitudes  $M_{1+}^{3/2}$ ,  $E_{1+}^{3/2}$ ,  $S_{1+}^{3/2}$ , which correspond to the  $P_{33}(1232)$  resonance, in the form of integral equations. In our analysis these amplitudes are presented as the solutions of these equations. They contain two parts: particular and homogeneous solutions. Particular solutions have definite magnitudes fixed by the Born term. Homogeneous solutions have definite shapes fixed by the integral equations and arbitrary weights which are fitted parameters in our analysis.

Due to the Watson theorem and large  $\pi N$  phases  $\delta_{0+}^{1/2}$  and  $\delta_{0+}^{3/2}$ , a significant contribution to the imaginary parts of the amplitudes in the  $P_{33}(1232)$  resonance region can also give nonresonant amplitudes  $E_{0+}^{(0)}$ ,  $E_{0+}^{1/2}$ ,  $E_{0+}^{3/2}$ ,  $S_{0+}^{(0)}$ ,

$S_{0+}^{1/2}$ , and  $S_{0+}^{3/2}$ . In order to find these amplitudes we have calculated their real parts by dispersion relations, taking into account the Born term and the  $P_{33}(1232)$  resonance contribution. Then the imaginary parts of the amplitudes were found using the Watson theorem with the phases  $\delta_{0+}^{1/2}$ ,  $\delta_{0+}^{3/2}$  taken from the analysis of the GWU(VPI) group [16, 17]. Above  $W = 1.3 GeV$ , these contributions were smoothly reduced to 0.

### B. Isobar models

For the isobar model approximation we used the approaches developed in Refs. [18, 19] with modifications made in Refs. [13, 14]. The main modification in the case of pion electroproduction is connected with the incorporation of Regge poles into the unitary isobar model of Ref. [18]. Due to this modification, the amplitudes of the model transform with increasing energies into the amplitudes in the Regge pole regime.

Isobar models contain the contributions of resonances parametrized in Breit-Wigner form, and nonresonant backgrounds built from the Born terms and the  $t$ -channel  $\rho$  and  $\omega$  contributions. In the case of pion production, the background is unitarized via unitarization of the multipole amplitudes in the  $K$ -matrix approximation. Below the two-pion production threshold, the background multipole amplitudes unitarized in this approximation satisfy the Watson theorem. At these energies, the Breit-Wigner formulas for the resonance contributions are modified in Ref. [13] in such a way that the resonance contributions to multipole amplitudes also satisfy the Watson theorem.

The Born terms play an important role in both approaches. They are determined by the coupling constant  $g_{\pi NN}$  which is well known, and  $g_{\eta NN}$  which we fix according to the results of the analysis of  $\eta$  photoproduction data in Ref. [14]. According to Ref. [18], in the unitary isobar model that we use for the analysis of  $\pi$  electroproduction, the  $\pi NN$  coupling being pseudovector at the threshold is transformed with increasing energy into pseudoscalar coupling. The parameter that describes this transition was fitted in our analysis; it turned out to be very close to the value found in Ref. [18].

The Born terms are determined also by the nucleon and pion form factors. We have parametrized these form factors in the following way. According to world data and taking into account recent measurements (see, for example, review [20]), we have parametrized proton form factors using the Bosted formulas [21]. The  $Q^2$  evolution of the neutron magnetic form factor we have described by the dipole formula  $G_d(Q^2) = 1/(1 + Q^2/0.71 GeV^2)^2$ , taking into account the observed deviation from this behaviour [20]. The value of the neutron electric form factor turned out to be very important for the simultaneous description of the  $\pi^+$  and  $\pi^0$  cross sections in the  $P_{33}(1232)$  resonance region. This form factor was obtained from the requirement of the best description of these data. As demonstrated below in Section IVA, the obtained values

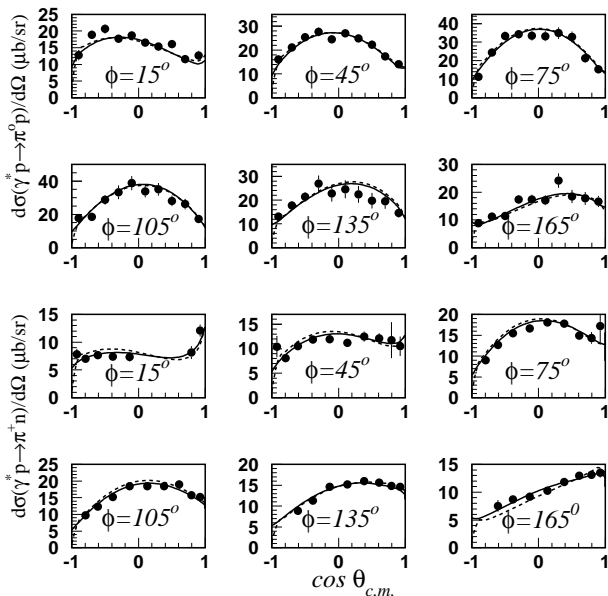


FIG. 1: Differential cross sections at  $Q^2 = 0.4$  ( $GeV/c$ )<sup>2</sup>:  $W = 1.22$   $GeV$  for  $\gamma^*p \rightarrow \pi^0p$  and  $W = 1.23$   $GeV$  for  $\gamma^*p \rightarrow \pi^+n$ . The solid and dashed curves are the results obtained using IM and DR, respectively. The data are from CLAS [8, 9].

are in good agreement with the results of recent measurements [22, 23, 24, 25]. The pion form factor was parametrized according to recent measurements [26] by the monopole formula  $1/(1 + Q^2/0.54 GeV^2)$ .

At  $Q^2 = 0$ , the  $\rho$  and  $\omega$  contributions were found in the analyses of  $\pi$  and  $\eta$  photoproduction data in Refs. [14, 18]. We have introduced the  $Q^2$  evolution of these contributions via the description of the  $\rho(\omega) \rightarrow \pi\gamma$  and  $\rho(\omega) \rightarrow \eta\gamma$  form factors using the dipole formula  $G_d(Q^2)$ . In order to take into account the uncertainty of these form factors, the  $\rho$  and  $\omega$  contributions were allowed to vary in the vicinity of their values found in the above described way. It turned out that the obtained deviations do not exceed 20%.

### III. DATA AND ANALYSIS

We have analyzed the following sets of data at  $Q^2 = 0.4$  and  $0.65$  ( $GeV/c$ )<sup>2</sup>.

(a) At  $Q^2 = 0.4$  ( $GeV/c$ )<sup>2</sup> the data used in our analysis are the results of recent CLAS measurements of  $\pi^0$  ( $W = 1.1 - 1.68$   $GeV$ ) [8] and  $\pi^+$  ( $W = 1.1 - 1.55$   $GeV$ ) [9] differential cross sections, and polarized beam asymmetry in  $\pi^0$  and  $\pi^+$  electroproduction ( $W = 1.1 - 1.66$   $GeV$ ) [11, 12].

(b) At  $Q^2 = 0.65$  ( $GeV/c$ )<sup>2</sup> we have used recent CLAS measurements of  $\pi^0$  electroproduction cross sections ( $W = 1.1 - 1.52$   $GeV$ ,  $E_e = 1.645$   $GeV$  and  $W = 1.1 - 1.68$   $GeV$ ,  $E_e = 2.445$   $GeV$ ) [8], and polarized beam asymmetry in  $\pi^0$  and  $\pi^+$  electroproduction ( $W =$

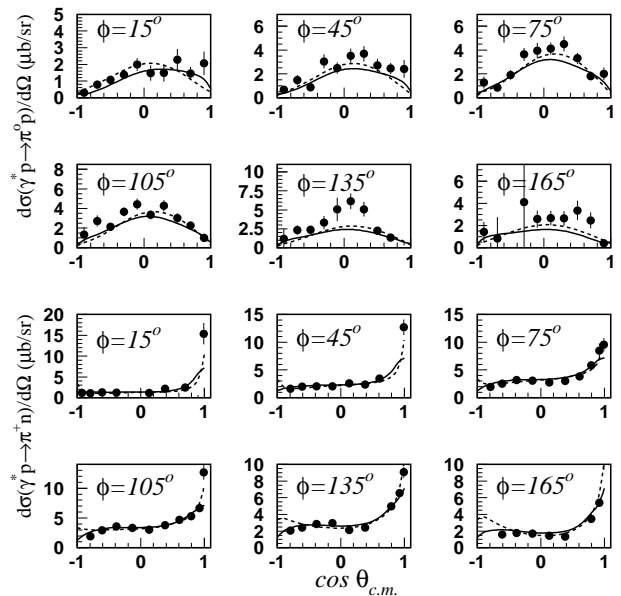


FIG. 2: Differential cross sections at  $Q^2 = 0.4$  ( $GeV/c$ )<sup>2</sup>:  $W = 1.52$   $GeV$  for  $\gamma^*p \rightarrow \pi^0p$  and  $W = 1.53$   $GeV$  for  $\gamma^*p \rightarrow \pi^+n$ . The solid and dashed curves are the results obtained using IM and DR, respectively. The data are from CLAS [8, 9].

$1.1 - 1.66$   $GeV$ ) [11, 12]. We have also used CLAS data on  $\pi^+$  differential cross sections ( $W = 1.1 - 1.41$   $GeV$ ,  $Q^2 = 0.6$  ( $GeV/c$ )<sup>2</sup>) [9]. As the values of  $Q^2$  in [9] and the main data set are different, and the data on  $\pi^+$  differential cross sections extend over more restricted range in  $W$ , we have complemented this data set by the results of DESY for  $\pi^0$  and  $\pi^+$  differential cross sections at  $W = 1.415 - 1.505$   $GeV$ ,  $Q^2 = 0.6 - 0.63$  ( $GeV/c$ )<sup>2</sup> [27, 28] and  $W = 1.565 - 1.655$   $GeV$ ,  $Q^2 = 0.6 - 0.64$  ( $GeV/c$ )<sup>2</sup> [29, 30], and by the results of NINA for  $\pi^0$  differential cross sections at  $W = 1.395 - 1.425$   $GeV$ ,  $Q^2 = 0.6, 0.61$  ( $GeV/c$ )<sup>2</sup> [31].

Let us note that unlike old measurements, which extend mostly over limited ranges of angles, the CLAS data cover the full angular range.

Both data sets include first, second, and partly third resonance regions. The full angular coverage of the CLAS data, and the presence of the  $A_{LT'}$  data, which are sensitive both to transverse and longitudinal amplitudes, allowed us to reliably evaluate the resonance contributions in the first and second resonance regions.

The analysis of old data has been performed in Ref. [32] with inclusion from data sets (a) and (b) only for  $\pi^0$  differential cross sections. The obtained results qualitatively agree with our's, however, there are significant differences in details, and in Ref. [32] the longitudinal helicity amplitude for the  $\gamma^*p \rightarrow D_{13}(1520)$  transition is not found. As shown below, in our analysis this amplitude is found with good accuracy.

The fitted parameters in our analysis were the magnitudes of the multipole amplitudes corresponding to

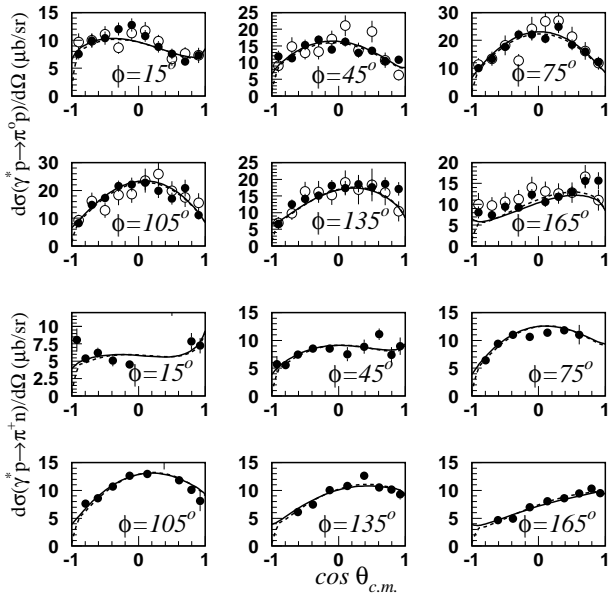


FIG. 3: Differential cross sections for  $\gamma^*p \rightarrow \pi^0 p$  at  $Q^2 = 0.65$  ( $GeV/c$ )<sup>2</sup> and  $W = 1.22$   $GeV$  and  $\gamma^*p \rightarrow \pi^+ n$  at  $Q^2 = 0.6$  ( $GeV/c$ )<sup>2</sup> and  $W = 1.23$   $GeV$ . The solid and dashed curves are the results obtained using IM and DR, respectively. The data are from CLAS [8, 9]. For  $\gamma^*p \rightarrow \pi^0 p$ , open and solid circles correspond to measurements with  $E_e = 1.645$  and  $2.445$   $GeV$  [8], respectively.

the contributions of the resonances from the first and second resonance regions at resonance positions. The magnitudes of the amplitudes corresponding to the most prominent resonance of the third resonance region, the  $F_{15}(1680)$ , were also fitted. The transverse amplitudes of the  $S_{31}(1620)$ ,  $S_{11}(1650)$ ,  $D_{15}(1675)$ ,  $D_{13}(1700)$  and  $D_{33}(1700)$  were fixed according to the results of the analysis made within the single quark transition model in Ref. [33]. The longitudinal amplitudes of these resonances and the amplitudes of other resonances were fixed taking into account the results obtained in the analysis in Ref. [34]. In order to check the stability of our results, we also performed an analysis where the amplitudes of all resonances from the third resonance region were also fitted. The obtained results for the amplitudes in the first and second resonance regions remained stable.

It is known that  $\eta$  photo- and electroproduction provide a unique opportunity to study the  $S_{11}(1535)$  resonance, because the contributions of nearby resonances are strongly suppressed in comparison with the  $S_{11}(1535)$  contribution. In order to obtain additional information on the electroexcitation of the  $S_{11}(1535)$ , we have also performed an analysis of the CLAS data on  $\eta$  electroproduction cross sections at  $Q^2 = 0.375$  ( $GeV/c$ )<sup>2</sup> ( $W = 1.5 - 1.62$   $GeV$ ) and  $Q^2 = 0.75$  ( $GeV/c$ )<sup>2</sup> ( $W = 1.5 - 1.83$   $GeV$ ) [10]. In our analysis of these data we have taken into account the results obtained in the analyses of  $\eta$  photoproduction in Ref. [14] and of  $\pi$  electroproduction in this work. The contributions of all resonances, ex-

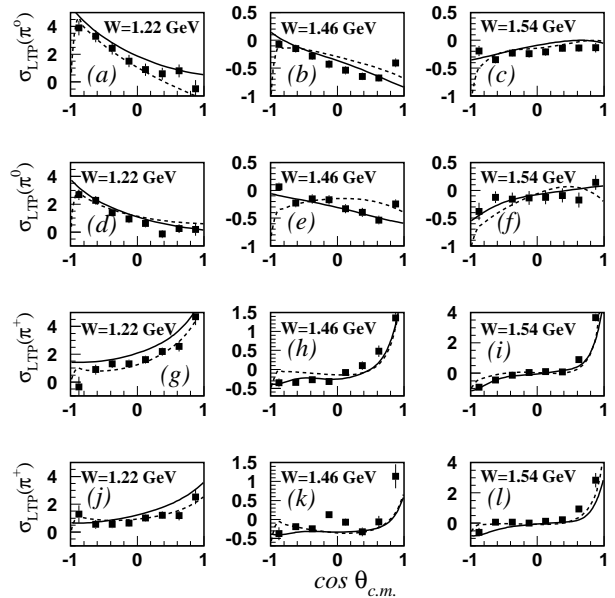


FIG. 4: Structure function  $\sigma_{LT'}$  for  $\gamma^*p \rightarrow \pi^0 p$  at  $Q^2 = 0.4$  ( $GeV/c$ )<sup>2</sup> (Figs. a-c) and  $Q^2 = 0.65$  ( $GeV/c$ )<sup>2</sup> (Figs. d-f), and for  $\gamma^*p \rightarrow \pi^+ n$  at  $Q^2 = 0.4$  ( $GeV/c$ )<sup>2</sup> (Figs. g-i) and  $Q^2 = 0.65$  ( $GeV/c$ )<sup>2</sup> (Figs. j-l). The solid and dashed curves are the results obtained using IM and DR, respectively. The data are from CLAS [11, 12].

Observable	$Q^2$	Number of data points		$\chi^2/data$	
		IM	DR	IM	DR
$\frac{d\sigma}{d\Omega}(\pi^0)$	0.4	3530	1.22	1.21	
	0.6-0.65	6537	1.22	1.39	
$\frac{d\sigma}{d\Omega}(\pi^+)$	0.4	2308	1.62	1.97	
	0.6-0.65	1716	1.48	1.75	
$A_{LT'}(\pi^0)$	0.4	956	1.14	1.25	
	0.65	805	1.07	1.3	
$A_{LT'}(\pi^+)$	0.4	918	1.18	1.63	
	0.65	812	1.18	1.15	
$\frac{d\sigma}{d\Omega}(\eta)$	0.375	172	1.32	1.33	
	0.75	412	1.42	1.45	

TABLE I: Obtained values of  $\chi^2$ .

cept the  $S_{11}(1535)$ , were fixed according to these results. With this, the  $\eta N$  branching ratios for the  $D_{13}(1520)$  and  $F_{15}(1680)$  were taken from Ref. [14]. Other  $\eta N$  branching ratios and the branching ratios to  $\pi N$  channel were taken from the RPP [15]. So, only the amplitudes of the  $S_{11}(1535)$  were fitted in our analysis of  $\eta$  data.

#### IV. RESULTS AND DISCUSSION

The results of our fit to the data are presented in Table I. The description is good for all observables in both approaches. The somewhat larger value of  $\chi^2$  for the  $\pi^+$  cross sections is associated with the small statistical un-

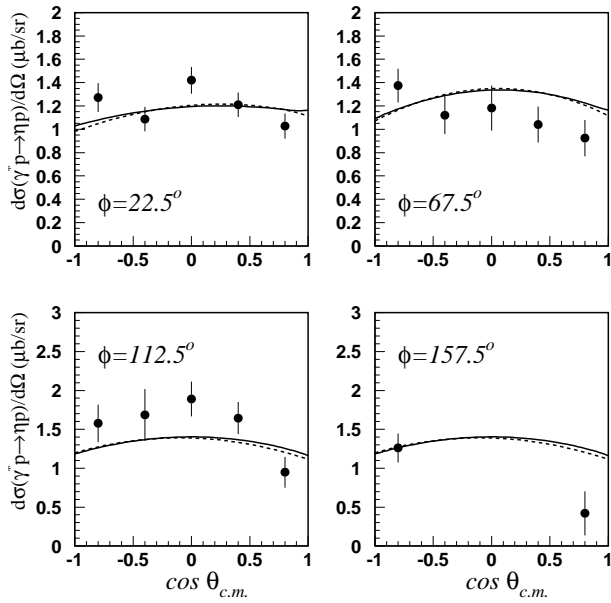


FIG. 5: Differential cross sections for  $\gamma^*p \rightarrow \eta p$  at  $Q^2 = 0.375 (GeV/c)^2$  and  $W = 1.53 GeV$ . The solid and dashed curves are the results obtained using IM and DR, respectively. The data are from CLAS [10].

certainties of these measurements [9]. In Figs. 1-6 we present our results for observables in comparison with experimental data.

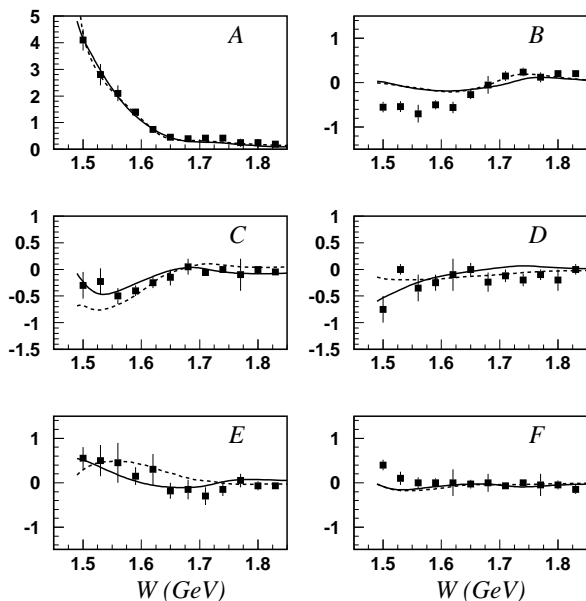


FIG. 6: Coefficients  $A, B, C, D, E, F$  at  $Q^2 = 0.75 (GeV/c)^2$  in the expansion of  $\gamma^*p \rightarrow \eta p$  differential cross section over  $\cos\theta$  [10]. The solid and dashed curves are the results obtained using IM and DR, respectively. The data are from CLAS [10].

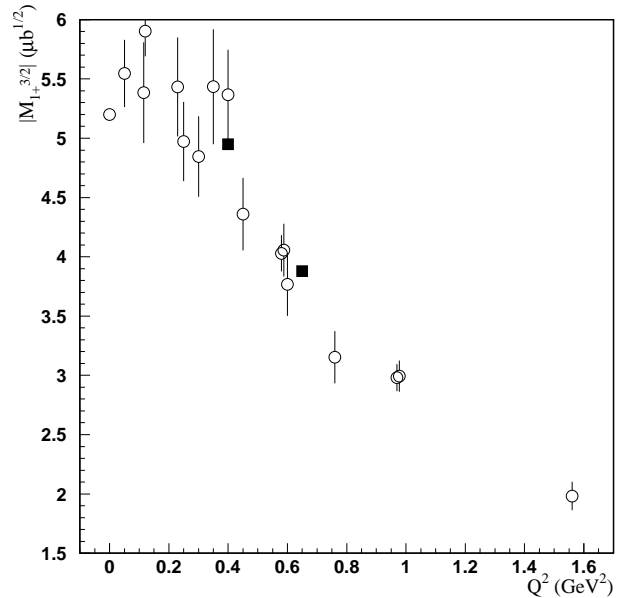


FIG. 7: The amplitude  $|M_{1+}^{3/2}|$  at  $W = 1.229 GeV$ , where according to the GWU(VPI) analysis of pion photoproduction [17, 35]  $ReM_{1+}^{3/2} = 0$ . Full boxes are the average values of our results obtained using IM and DR. Open circles correspond to Refs. [36, 37, 38, 39, 40]. Open circle at  $Q^2 = 0$  is the result of the GWU(VPI) analysis of pion photoproduction data [17, 35].

### A. $P_{33}(1232)$

The  $P_{33}(1232)$  is an isolated resonance located in the region where the corresponding  $\pi N$  amplitude is elastic. For this reason, the  $P_{33}(1232)$  is investigated with great accuracy in  $\pi N$  scattering and in  $\pi$  photoproduction. Due to isotopic invariance violation and possible presence of nonresonant contributions, there is a difference between the phases  $\delta_{1+}^{3/2}$  found in these reactions. According to the analyses of the GWU(VPI) group [16, 17, 35], the value of  $W$ , where  $\delta_{1+}^{3/2} = \pi/2$ , is  $\simeq 1.232 GeV$  in  $\pi N$  scattering, and  $\simeq 1.229 GeV$  in  $\pi$  photoproduction. In our analysis we have used the phase  $\delta_{1+}^{3/2}$  found in the GWU(VPI) analysis of pion photoproduction, and the amplitudes presented in Table II correspond to  $W = 1.229 GeV$ . We have checked the possibility of shifting this phase; however, in both approaches this was not supported by the fit to the data.

From Table II it can be seen that the amplitudes obtained in the two analyses are in good agreement with each other. The values of the ratios  $ImE_{1+}^{3/2}/ImM_{1+}^{3/2}$ ,  $ImS_{1+}^{3/2}/ImM_{1+}^{3/2}$  are well determined, and are in good agreement with the results of Ref. [8] obtained from  $\pi^0$  cross sections using a multipole expansion.

In Fig. 7 we compare our results for  $M_{1+}^{3/2}$  with the values obtained in coincidence  $\pi^0$  electroproduction experiments [36, 37, 38, 39, 40] using multipole analysis. Significantly smaller uncertainties are obtained from the

new CLAS data.

There are also the values of  $M_{1+}^{3/2}$  obtained in inclusive experiments [41, 42, 43]. Our analysis shows that these values are in very good agreement with our results. However, the  $M_{1+}^{3/2}$  amplitudes obtained from inclusive data are not very reliable, as no partial-wave analysis is possible in this case, and the separation of the transverse and longitudinal contributions in these measurements is arbitrary. For this reason we do not present here the comparison with the results obtained in inclusive experiments.

It is interesting to note that the possibility of simultaneously describing the  $\pi^0$  and  $\pi^+$  electroproduction cross sections in the  $P_{33}(1232)$  resonance region depends significantly on the value of the neutron electric form factor  $G_{en}(Q^2)$ , which enters  $\gamma^*p \rightarrow \pi^+n$  through the  $u$  channel neutron exchange. This form factor gives significant contribution to the multipole  $E_{0+}(\gamma^*p \rightarrow \pi^+n)$ , which has a large contribution to  $\pi^+$  electroproduction cross section at  $W < 1.3$  GeV. For example,  $G_{en}(Q^2) = 0.06$  reduces  $E_{0+}(\gamma^*p \rightarrow \pi^+n)$  at  $Q^2 = 0.4$  and  $W = 1.23$  GeV by 13 %. By this reason  $G_{en}(Q^2)$  significantly affects the value of the resonance multipole amplitude  $M_{1+}^{3/2}$  which is needed to describe  $\pi^+$  electroproduction cross section in the  $P_{33}(1232)$  resonance region. In both our approaches we have found that a successful simultaneous description of the  $\pi^0$  and  $\pi^+$  electroproduction cross sections requires values of  $G_{en}(Q^2) = 0.06$  and  $0.05$  at  $Q^2 = 0.4$  and  $0.65$  (GeV/c)<sup>2</sup>, respectively. These values are in good agreement with the results of recent measurements:  $G_{en}(Q^2) = 0.052 \pm 0.004$  [22] at  $Q^2 = 0.4$  (GeV/c)<sup>2</sup>,  $G_{en}(Q^2) = 0.046 \pm 0.006 \pm 0.003$  [23],  $G_{en}(Q^2) = 0.053 \pm 0.003 \pm 0.003$  [25] at  $Q^2 = 0.5$  (GeV/c)<sup>2</sup>, and  $G_{en}(Q^2) = 0.048 \pm 0.007$  [24] at  $Q^2 = 0.67$  (GeV/c)<sup>2</sup>.

### B. $P_{11}(1440)$ , $D_{13}(1520)$ , $S_{11}(1535)$

The results for these resonances are presented in Tables III and IV. The quoted errors are the uncertainties arising from the fitting procedure. Comparison of the results obtained in the two approaches allows us to estimate the model dependence of the extracted amplitudes. It is seen that the two approaches give very close results, except for the transverse helicity amplitude for the  $P_{11}(1440)$  electroexcitation where the difference of the results obtained using the two approaches is significantly larger than the fit uncertainties. Nevertheless, we can make definite conclusion that the  $A_{1/2}$  amplitude of the  $\gamma^*p \rightarrow P_{11}(1440)$  transition falls very rapidly in comparison with its value at  $Q^2 = 0$ .

In Figs. 8-9 we present our results for the helicity amplitudes of the  $\gamma^*p \rightarrow P_{11}(1440)$ ,  $D_{13}(1520)$ , and  $S_{11}(1535)$  transitions along with the results at the photon point from the RPP [15], where the outcomes of various analyses are combined. Separately, at  $Q^2 = 0$ , we present the results for the  $S_{11}(1535)$  found in  $\pi$  [16] and

$\eta$  [14] photoproduction. At  $Q^2 > 0$ , data on helicity amplitudes are more sparse and available only for the  $D_{13}(1520)$ ,  $S_{11}(1535)$  transverse amplitudes. These data are analyzed in Ref. [33] on the basis of the single quark transition model. As a result, bands that correspond to the existing data from Bonn, DESY, and NINA, and JLab measurements of  $\eta$  electroproduction [10] are found. These bands are presented in Figs. 8-9 in the form of shadowed areas.

From Figs. 8-9 it is seen that our results for the  $D_{13}(1520)$  and  $S_{11}(1535)$  transverse amplitudes are in good agreement with the results that follow from the previous data. It should be noted, however, that our results give a much more definite value for the  ${}_pA_{1/2}$  amplitude of the  $\gamma^*p \rightarrow D_{13}(1520)$  transition than earlier results. The transverse amplitude  ${}_pA_{3/2}$  for this transition, which is dominant at  $Q^2 = 0$ , falls very rapidly with increasing  $Q^2$ , and all quark models predict that at high  $Q^2$ ,  ${}_pA_{1/2}$  will become the dominant contribution to  $\gamma^*p \rightarrow D_{13}(1520)$ . Such behavior is confirmed by our analysis of the CLAS data, with the crossover where  ${}_pA_{1/2} = {}_pA_{3/2}$  occurring around  $Q^2 = 0.4 - 0.65$  (GeV/c)<sup>2</sup>.

From Fig. 8 it is seen that the transverse helicity amplitude  ${}_pA_{1/2}$  of the  $P_{11}(1440)$  shows a rapid fall off with  $Q^2$ . Moreover, at  $Q^2 \simeq 0.5 - 0.6$  (GeV/c)<sup>2</sup> this amplitude, apparently, changes sign.

Amplitudes corresponding to the  $S_{11}(1535)$  have been investigated in our analysis of  $\pi$  and  $\eta$  electroproduction. For consistent comparison of these amplitudes and for comparison with the results obtained in other works, following Ref. [10], we have used the parameters:  $M = 1530$  MeV,  $\Gamma_{tot} = 150$  MeV,  $\beta_{\pi N} = 0.4$  and  $\beta_{\eta N} = 0.55$ . It is seen that unlike at  $Q^2 = 0$ , where the amplitude  ${}_pA_{1/2}$  found in  $\pi$  photoproduction is much smaller than the amplitude found in  $\eta$  photoproduction, our results for  $\pi$  and  $\eta$  electroproduction are in good agreement with each other.

In Figs. 8-9 we compare our results with quark model predictions. As mentioned in the Introduction, with increasing  $Q^2$  a relativistic treatment of the electroexcitations of the nucleon resonances becomes essential. The most appropriate way to realize this is to consider electromagnetic transition amplitudes in the light-front dynamics (see, for example, Refs. [44, 45, 46]). Such an approach has been used to investigate the  $Q^2$  evolution of the  $\gamma^*p \rightarrow P_{11}(1440)$ ,  $D_{13}(1520)$ , and  $S_{11}(1535)$  transitions in Ref. [46]. From the results of this investigation the important role of relativistic effects is quite evident: bold and thin solid curves in Figs. 8-9 correspond to relativistic and nonrelativistic calculations. Light-front dynamics has also been used in Refs. [47, 48] for investigation of the  $\gamma^*p \rightarrow P_{11}(1440)$ ,  $S_{11}(1535)$  transition amplitudes. Different forms of interquark forces inspired by QCD are considered in Refs. [49, 50], where the relativistic effects are taken into account only partly. From Figs. 8-9 it can be seen that none of the approaches [46, 47, 48, 49, 50] gives simultaneously a good description of the  $\gamma^*p \rightarrow P_{11}(1440)$ ,  $D_{13}(1520)$ ,  $S_{11}(1535)$  tran-

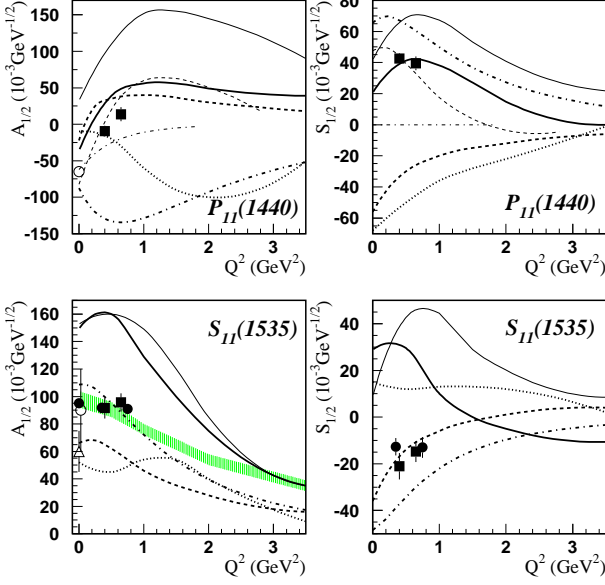


FIG. 8: Helicity amplitudes for the  $P_{11}(1440)$  and  $S_{11}(1535)$  electroexcitations on protons. Full boxes are the average values of our results obtained in the analysis of  $\pi$  electroproduction data using IM and DR. Full circles are the average values of the results obtained using IM and DR in the analysis of  $\eta$  photo and electroproduction data in Ref. [14] and in this work. Open triangle at  $Q^2 = 0$  is the result of the GWU(VPI) analysis of pion photoproduction data [16]. Open circles at  $Q^2 = 0$  are the RPP estimates [15]. Shaded area [33] corresponds to the results obtained from the existing Bonn, DESY, and NINA data, and from JLab measurements of  $\eta$  electroproduction [10]. Bold and thin solid curves correspond to relativistic and nonrelativistic quark model calculations in Ref. [46]. Bold dashed curves correspond to the light-front calculations of Refs. [47, 48]. Dotted, bold dashed-dotted and thin dashed curves correspond to the quark models of Refs. [49, 50, 51]. Thin dashed-dotted curves are the predictions obtained assuming that the  $P_{11}(1440)$  is a  $q^3G$  hybrid state [1].

sition amplitudes.

In Ref. [51] for the  $\gamma^*p \rightarrow P_{11}(1440)$  transition, the contribution of the diagram where the photon interacts with the  $q\bar{q}$  cloud of the nucleon is taken into account in addition to the main mechanism where electroexcitation of the nucleon occurs via photon interaction with constituent quarks. From Fig. 8 it can be seen that the predictions of Ref. [51] are qualitatively similar to the results of the light-front approach [46] and are in good agreement with our results. However, for definite conclusions it is necessary to also have predictions of the Ref. [51] approach for the  $\gamma^*p \rightarrow D_{13}(1520)$ ,  $S_{11}(1535)$  transitions.

In Fig. 8 we have also presented the predictions for the  $P_{11}(1440)$  obtained by assuming that the  $P_{11}(1440)$  is a  $q^3G$  hybrid state [1]. It is seen that the longitudinal helicity amplitude of the  $\gamma^*p \rightarrow P_{11}(1440)$  transition obtained under this assumption strongly contradicts our results.

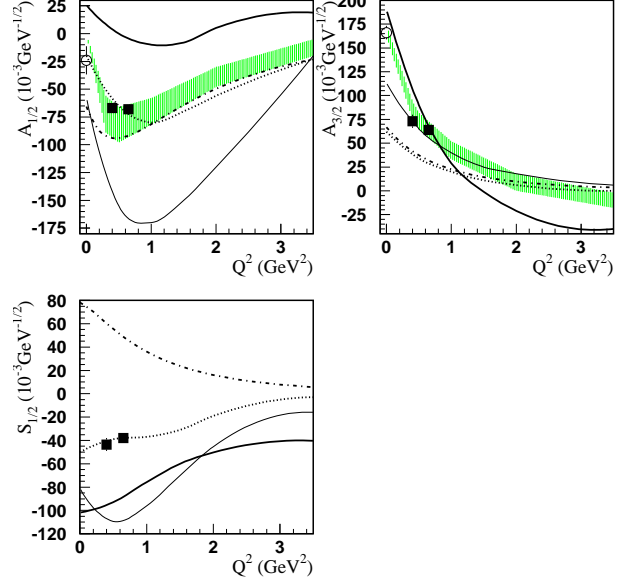


FIG. 9: Helicity amplitudes for the  $D_{13}(1520)$  electroexcitation. All other relevant information is as given in the legend for Figure 8.

In Figs. 5-6 we present our results for  $\eta$  electroproduction in comparison with experimental data. In Fig. 5 the results are presented for differential cross sections at  $Q^2 = 0.375 (GeV/c)^2$  and  $W = 1.53 GeV$ . The data have some forward-backward asymmetry which has not been seen in photoproduction data and is not reproduced by our present analysis. In Fig. 6 the data at  $Q^2 = 0.75 (GeV/c)^2$  are presented in the form of coefficients  $A, B, C, D, E, F$  in the expansion of the differential cross section over  $\cos\theta$ , where  $\theta$  is the polar angle [10]. The agreement with the data is good everywhere, except for  $B$  below  $W = 1.65 GeV$ . The coefficient  $B$  and the forward-backward asymmetry in the cross section come from interference between  $S_{11}$  and  $P_{11}$  waves, and the analysis shows that the contribution  $\simeq 0.2 \mu b^{1/2}$  is required in the  $ImM_{1-}$  in the  $S_{11}(1535)$  resonance region for both values of  $Q^2 = 0.375$  and  $0.75 (GeV/c)^2$ . Such contribution is excluded by photoproduction data. Our estimations show that the contribution  $\simeq 0.2 \mu b^{1/2}$  to  $ImM_{1-}$  can not be explained by  $\gamma^*p \rightarrow \pi N \rightarrow \eta p$  and  $\gamma^*p \rightarrow \eta p \rightarrow \eta p$ , i.e., by final state interactions effects. Due to its large width, the tail of the  $P_{11}(1440)$  can, in principle, contribute to the  $ImM_{1-}$  above the  $\eta p$  production threshold. However, in this case one needs an unrealistically large coupling constant  $F_2^R(Q^2)$  for the  $\gamma^*N \rightarrow P_{11}(1440)$  transition (notations of Ref. [14]), by an order of magnitude larger than in  $\pi$  electroproduction and in  $\eta$  photoproduction [14]. Therefore, there is no common explanation of the forward-backward asymmetry in the electroproduction data, and the consistency of photo- and electroproduction data should be checked.

$Q^2$ ( $GeV/c$ ) <sup>2</sup>	$ImM_{1+}^{3/2}$ ( $\mu b^{1/2}$ )	$ImE_{1+}^{3/2}/ImM_{1+}^{3/2}$ (%)	$ImS_{1+}^{3/2}/ImM_{1+}^{3/2}$ (%)	Approach
0.4	$4.93 \pm 0.01$	$-2.4 \pm 0.2$	$-5.0 \pm 0.2$	IM
	$4.97 \pm 0.01$	$-2.9 \pm 0.2$	$-5.9 \pm 0.2$	DR
		$-3.4 \pm 0.4 \pm 0.4$	$-5.6 \pm 0.4 \pm 0.6$	[8]
0.65	$3.87 \pm 0.01$	$-1.0 \pm 0.3$	$-6.2 \pm 0.4$	IM
	$3.89 \pm 0.01$	$-2.0 \pm 0.3$	$-7.0 \pm 0.4$	DR
		$-1.9 \pm 0.5 \pm 0.5$	$-6.9 \pm 0.6 \pm 0.5$	[8]
		$-2.0 \pm 0.4 \pm 0.4$	$-6.6 \pm 0.4 \pm 0.2$	[8]

TABLE II: The results for the imaginary parts of  $M_{1+}^{3/2}$ ,  $E_{1+}^{3/2}$ ,  $S_{1+}^{3/2}$  at  $W = 1.229$   $GeV$ . The results on the third and fourth rows are obtained in Ref. [8] using a truncated multipole expansion.

## V. SUMMARY

We present in this paper the results of our analysis of recent CLAS data on  $\pi$  and  $\eta$  electroproduction [8, 9, 10, 11, 12]. High precision of the data in combination with their full angular coverage, the existence of longitudinally polarized beam asymmetry data and utilization of two approaches, allowed us to obtain accurate results for the photocoupling transition amplitudes of the  $P_{33}(1232)$ ,  $P_{11}(1440)$ ,  $D_{13}(1520)$ , and  $S_{11}(1535)$  electroexcitation on the proton.

- For the first time definite results are obtained for the longitudinal amplitudes of the transitions  $\gamma^*p \rightarrow P_{11}(1440)$ ,  $D_{13}(1520)$ , and  $S_{11}(1535)$ .
- The values obtained for the ratios  $ImE_{1+}^{3/2}/ImM_{1+}^{3/2}$ ,  $ImS_{1+}^{3/2}/ImM_{1+}^{3/2}$  for the  $P_{33}(1232)$  contribution at the resonance position are in good agreement with the results of Ref. [8] obtained from  $\pi^0$  cross sections using a truncated multipole expansion.
- We have found that the value of the neutron electric form factor is very important for the simultaneous description of the  $\pi^+$  and  $\pi^0$  cross sections in the  $P_{33}(1232)$  resonance region. The obtained values are in good agreement with the results of recent direct measurements [22, 23, 24, 25].
- The photocoupling amplitudes for the  $\gamma^*p \rightarrow S_{11}(1535)$  transition extracted separately from the analysis of  $\pi$  and  $\eta$  electroproduction are in good agreement.

- The transverse amplitude of the  $\gamma^*p \rightarrow P_{11}(1440)$  transition falls very rapidly with increasing  $Q^2$ , and, apparently, changes sign at  $Q^2 \simeq 0.5 - 0.6$  ( $GeV/c$ )<sup>2</sup>.
- Our results show a strong longitudinal response for the  $P_{11}(1440)$ ; thus, they rule out presentation of this resonance as a  $q^3G$  hybrid state.
- Absolute values of the transverse amplitudes  ${}_pA_{1/2}$  and  ${}_pA_{3/2}$  of the  $\gamma^*p \rightarrow D_{13}(1520)$  transition become equal to each other at  $Q^2 = 0.4 - 0.65$  ( $GeV/c$ )<sup>2</sup>.
- Comparison of our results with the existing quark model predictions show that none simultaneously gives a good description of the  $\gamma^*p \rightarrow P_{11}(1440)$ ,  $D_{13}(1520)$ ,  $S_{11}(1535)$  transition amplitudes.
- In the analysis of  $\eta$  electroproduction in the  $S_{11}(1535)$  resonance region, we have found it necessary to introduce a large  $P_{11}$  contribution which is not seen in photoproduction data and is not related to the  $P_{11}(1440)$  resonance.

We are grateful to D. Richards for discussions of lattice results, to V. Mokeev for useful discussions, to I. Strakovski for his help in getting data from SAID database, and to M. M. Giannini for providing us the results of their quark model predictions. I. G. Aznauryan expresses her gratitude for the hospitality at Jefferson Lab.

- 
- [1] Z. Li, V. Burkert, and Z. Li, Phys. Rev. **D46**, 70 (1992).
  - [2] N. Kaiser, P. B. Siegel, and W. Weise, Phys. Lett. **B362**, 23 (1995).
  - [3] Z. Li and R. L. Workman, Phys. Rev. **C53**, 549 (1996).
  - [4] M. Göckeler, T. R. Hemmert, R. Horsley et al, hep-lat/0303019.
  - [5] C. Alexandrou, Ph. de Forcrand, Th. Lippert et al, Phys. Rev. **D69**, 114506 (2004).
  - [6] C. Alexandrou, Ph. de Forcrand, H. Neff et al, hep-lat/0409122.



	$Q^2$ [(GeV/c) <sup>2</sup> ]	${}_pE_{0+}^{1/2}$ ( $\mu b^{1/2}$ )	${}_pS_{0+}^{1/2}$ ( $\mu b^{1/2}$ )	${}_pA_{1/2}$ ( $10^{-3} GeV^{-1/2}$ )	${}_pS_{1/2}$ ( $10^{-3} GeV^{-1/2}$ )	Approach
$\gamma^* p \rightarrow \pi N$	0.4	$0.56 \pm 0.01$	$-0.20 \pm 0.02$	$95 \pm 2$	$-25 \pm 2$	IM
		$0.52 \pm 0.02$	$-0.15 \pm 0.02$	$88 \pm 4$	$-18 \pm 2$	DR
	0.65	$0.58 \pm 0.02$	$-0.14 \pm 0.02$	$98 \pm 4$	$-17 \pm 2$	IM
		$0.55 \pm 0.02$	$-0.1 \pm 0.02$	$93 \pm 4$	$-12 \pm 2$	DR
$\gamma^* p \rightarrow \eta p$	0.375	$1.79 \pm 0.02$	$-0.33 \pm 0.07$	$92 \pm 1$	$-12 \pm 3$	IM
		$1.77 \pm 0.02$	$-0.36 \pm 0.08$	$91 \pm 1$	$-13 \pm 3$	DR
	0.75	$1.73 \pm 0.02$	$-0.32 \pm 0.08$	$89 \pm 1$	$-12 \pm 3$	IM
		$1.80 \pm 0.02$	$-0.38 \pm 0.08$	$93 \pm 1$	$-14 \pm 3$	DR

TABLE III: The  $S_{11}(1535)$  amplitudes obtained in the analyses of  $\pi$  and  $\eta$  electroproduction. Helicity amplitudes for the  $S_{11}(1535)$  electroexcitation are obtained using  $M = 1530 MeV$ ,  $\Gamma_{tot} = 150 MeV$ ,  $\beta_{\pi N} = 0.4$ ,  $\beta_{\eta N} = 0.55$ .

Resonance	$Q^2$	${}_pM_{l-}^{1/2}$	${}_pE_{l-}^{1/2}$	${}_pS_{l-}^{1/2}$	${}_pA_{1/2}$	${}_pA_{3/2}$	${}_pS_{1/2}$	Approach
$P_{11}(1440)$	0.4	$0.07 \pm 0.01$		$0.31 \pm 0.01$	$-15 \pm 2$		$44 \pm 2$	IM
		$0.02 \pm 0.01$		$0.29 \pm 0.01$	$-4 \pm 2$		$41 \pm 2$	DR
	0.65	$-0.02 \pm 0.02$		$0.31 \pm 0.02$	$4 \pm 4$		$44 \pm 4$	IM
		$-0.11 \pm 0.02$		$0.26 \pm 0.02$	$23 \pm 4$		$37 \pm 4$	DR
$D_{13}(1520)$	0.4	$0.28 \pm 0.01$	$0.15 \pm 0.01$	$-0.17 \pm 0.01$	$-66 \pm 3$	$71 \pm 4$	$-46 \pm 3$	IM
		$0.29 \pm 0.01$	$0.16 \pm 0.01$	$-0.15 \pm 0.01$	$-68 \pm 3$	$75 \pm 3$	$-41 \pm 3$	DR
	0.65	$0.27 \pm 0.01$	$0.11 \pm 0.01$	$-0.14 \pm 0.01$	$-67 \pm 3$	$62 \pm 4$	$-38 \pm 3$	IM
		$0.28 \pm 0.01$	$0.12 \pm 0.01$	$-0.14 \pm 0.01$	$-69 \pm 3$	$66 \pm 4$	$-38 \pm 3$	DR

TABLE IV: Amplitudes of the  $P_{11}(1440)$  and  $D_{13}(1520)$  obtained in the analysis of  $\pi$  electroproduction. Multipole amplitudes are in  $\mu b^{1/2}$  units, helicity amplitudes are in  $10^{-3} GeV^{-1/2}$  units. Helicity amplitudes for the  $P_{11}(1440)$  electroexcitation are obtained using  $M = 1440 MeV$ ,  $\Gamma_{tot} = 350 MeV$ ,  $\beta_{\pi N} = 0.6$ . Helicity amplitudes for the  $D_{13}(1520)$  electroexcitation are obtained using  $M = 1520 MeV$ ,  $\Gamma_{tot} = 120 MeV$ ,  $\beta_{\pi N} = 0.5$ .

- [7] N. Mathur, S. J. Dong, T. Draper et al, hep-ph/0306199.  
[8] K. Joo et al., CLAS Collaboration, Phys. Rev. Lett. **88**, 122001 (2002).  
[9] H. K. Egiyan et al., CLAS Collaboration, to be submitted to Phys. Rev. C; L. C. Smith (for CLAS Collaboration), talk presented at NSTAR2004, Grenoble, France, March 24-27, 2004.  
[10] R. Thompson et al., CLAS Collaboration, Phys. Rev. Lett. **86**, 1702 (2001).  
[11] K. Joo et al., CLAS Collaboration, Phys. Rev. **C70**, 042201 (2004).  
[12] K. Joo et al., CLAS Collaboration, Phys. Rev. **C68**, 032201 (2003).  
[13] I. G. Aznauryan, Phys. Rev. **C67**, 015209 (2003).  
[14] I. G. Aznauryan, Phys. Rev. **C68**, 065204 (2003).  
[15] S. Eidelman et al., Phys. Lett. **B592**, 1 (2004).  
[16] R. A. Arndt, I. I. Strakovski, R. L. Workman, Phys. Rev. **C53**, 430 (1996).  
[17] R. A. Arndt, I. I. Strakovski, R. L. Workman, <http://gwdac.phys.gwu.edu>.  
[18] D. Drechsel, O. Hanstein, S. S. Kamalov, and L. Tiator, Nucl. Phys. **A645**, 145 (1999).  
[19] Wen-Tai Chiang, Shin Nan Yang, L. Tiator, and D. Drechsel, Nucl. Phys. **A700**, 429 (2002).  
[20] E. J. Brash, Proceedings of the 9th Int. Conf. on the Structure of Baryons "Baryons 2002", p. 256.  
[21] P. Bosted et al., Phys. Rev. **C51**, 718 (1995).  
[22] J. Golak et al., Phys. Rev. **C63**, 034006 (2001).  
[23] H. Zhu et al., Phys. Rev. Lett. **87**, 081801 (2001).  
[24] J. Bermuth et al., Phys. Lett. **B564**, 199 (2003).  
[25] G. Warren, Phys. Rev. Lett. **92**, 042301 (2004).  
[26] H. P. Blok et al., nucl-ex/0208011.  
[27] J. C. Alder et al., Nucl. Phys. **B105**, 253 (1976).  
[28] J. C. Alder et al., Nucl. Phys. **B99**, 1 (1975).  
[29] Ch. Gerhardt et al., Preprint DESY-F21-73/3 (1971)  
[30] Ch. Gerhardt et al., Preprint DESY-F21-79/02 (1979)  
[31] W. J. Shuttleworth et al., Nucl. Phys. **B45**, 428 (1972).  
[32] L. Tiator et al., Eur. Phys. Jour. **A19**, Suppl. **1**, 55 (2004).  
[33] V. D. Burkert et al., Phys. Rev. **C67**, 035204 (2003).  
[34] R. C. E. Devenish and D. H. Lyth, Nucl. Phys. **B93**, 109 (1975).  
[35] R. A. Arndt, W. J. Briscoe, I. I. Strakovski, R. L. Workman, Phys. Rev. **C66**, 055213 (2002).  
[36] W. W. Ash et al., Phys. Lett. **B24**, 165 (1967).

- [37] C. Mistretta et al., Phys. Rev. **184**, 1487 (1969).
- [38] W. Albrecht et al., Nucl. Phys. **B27**, 102 (1971).
- [39] R. Siddle et al., Nucl. Phys. **B35**, 93 (1971).
- [40] J. C. Alder et al., Nucl. Phys. **B46**, 573 (1972).
- [41] W. Bartel et al., Phys. Lett. **B28**, 148 (1968).
- [42] K. Bätzner et al., Phys. Lett. **B39**, 575 (1972).
- [43] S. Stein et al., Phys. Rev. **D12**, 1884 (1975).
- [44] I. G. Aznauryan, A. S. Bagdasaryan, and N. L. Ter-Isaakyan, Phys. Lett. **B112**, 393 (1982).
- [45] I. G. Aznauryan, Phys. Lett. **B316**, 391 (1993).
- [46] S. Capstick and B. D. Keister, Phys. Rev. **D51**, 3598 (1995).
- [47] E. Pace, G. Salme and S. Simula, Few Body Syst. Suppl. **10**, 407 (1999).
- [48] S. Simula, Proceedings of the Workshop on The Physics of Excited Nucleons, NSTAR 2001, p.135.
- [49] M. Warns, H. Schröder, W. Pfeil, and H. Rollnik, Z. Phys. C-Particles and Fields, **45**, 627 (1990).
- [50] M. Aiello, M. M. Giannini, and E. Santopinto, J. Phys. G:Nucl. Part. Phys., **24**, 753 (1998).
- [51] F. Cano and P. González, Phys. Lett. **B431**, 270 (1998).